

Magnetic response of $Y_{0.47}Pr_{0.53}Ba_2Cu_3O_{7-\delta}$: Superconductivity, glassiness, and paramagnetismV. Sandu,* P. Gyawali, T. Katuwal, and C. C. Almasan
Department of Physics, Kent State University, Kent, Ohio 44242, USA

B. J. Taylor and M. B. Maple

Department of Physics, University of California at San Diego, La Jolla, California 92093, USA
(Received 27 June 2006; revised manuscript received 19 September 2006; published 9 November 2006)

The magnetic response of the strongly underdoped $Y_{0.47}Pr_{0.53}Ba_2Cu_3O_{7-\delta}$ was investigated. We found the presence of superconducting and magnetic orders deep into the paramagnetic state, up to 200 K, which manifest as diamagneticlike response and hysteresis, respectively. We propose that the main source of irreversibility in this T range is the softening and melting of the glassy state into a viscous liquid of entities that behave like superparamagnetic particles with antiferromagnetic cores.

DOI: 10.1103/PhysRevB.74.184511

PACS number(s): 72.20.My

I. INTRODUCTION

Cuprate superconductors emerge from Mott insulators by doping. The effect of doping is nontrivial and, at 0 K, the quantum fluctuations generate criticality hence transitions between a couple of phases with different competing or coexisting orders. At finite temperatures, close to each quantum critical point, the dynamic properties of the system are anomalous reflecting, by continuity, the features of the competing orders. This picture is generally valid for all cuprates, but each system has a specific intermediate phase structure which, for most of the cuprates, is still under debate.

By far, the most investigated system is $La_{2-x}Sr_xCuO_4$. In this system, between the antiferromagnetic (AFM) and superconducting (SC) phases, the doping generates an insulating state with frozen short-range magnetic order (cluster spin glass).¹⁻⁵ This glassy state survives even at increased doping levels, at which the superconducting order becomes dominant.⁶⁻⁸

In the case of the bilayer $YBa_2Cu_3O_{6+x}$, the nature of the phases on the underdoped side of the superconducting dome is still controversial. Initially, it was suggested that AFM and SC phases meet at a quantum critical point.⁹⁻¹¹ Sutherland *et al.*¹² have interpreted the heat conductivity data in terms of an intermediate state between the AFM and SC states that is characterized by delocalized fermionic excitations. Additionally, neutron-scattering experiments have shown strong dynamic antiferromagnetic correlations deep into the SC state.¹⁰ Moreover, Sanna *et al.*¹³ claim, based on muon spin relaxation (μ SR) data, the existence of stripelike AFM and SC domains for strongly underdoped but superconducting samples ($x=0.4$), with the AFM domains, however, small enough to be “transparent” to the SC ordering. Nevertheless, it was demonstrated that the unusual commensurate AFM phase (in plane staggered moment $\approx 0.05\mu_B$) is subcritical and fluctuates on a nanosecond time scale.^{14,15}

The Pr substitution for Y in $Y_{1-x}Pr_xBa_2Cu_3O_{7-\delta}$ seems to be a special case. For optimal oxygen doping, Pr has an antidoping effect as a result of the hybridization of the f - p orbitals, pushing the system outside the SC dome for $x \geq 0.55$. Early investigations on this system have concluded that SC emerges directly from the AFM state at $x_c=0.55$ without any intermediate phase.¹⁶⁻¹⁸ However, μ SR

experiments¹⁷ have shown that short-range magnetic correlations are present inside the superconducting dome (for $x=0.4 \leq x_c$).

A phase diagram for $Y_{1-x}Pr_xBa_2Cu_3O_{7-\delta}$ is shown in Fig. 1, in which the charge-carrier dependence of the superconducting transition temperature T_c of the single crystals measured by us,¹⁹ and of the Néel temperatures of Cu and Pr sublattices, from data by Cooke *et al.*,¹⁸ are plotted. Above the lines delimiting the low-symmetry states, i.e., SC and AFM, a paramagnetic state is predicted by mean-field theory. However, at low carrier concentrations, in the crossover region of the SC and AFM phases, the strong fluctuations of the competing orders could extend far into the paramagnetic state and affect the magnetic response of the sample.

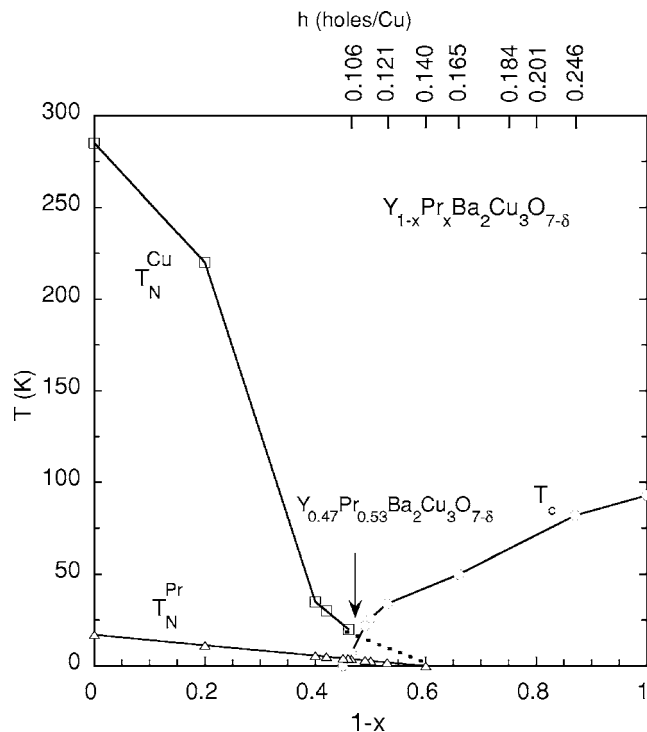


FIG. 1. Hole doping $1-x$, proportional with the number of carriers h , dependence of the Néel temperatures of Cu and Pr sublattices (from Ref. 18), and the superconducting transition temperature T_c (from Ref. 19). The solid lines are guides to the eye.

In this paper we investigate the magnetic response of $Y_{0.47}Pr_{0.53}Ba_2Cu_3O_{7-\delta}$ using long-time t_m experimental techniques such as dc magnetization ($t_m \approx 1-10$ sec) and ac-susceptibility ($t_m \approx 10^{-3}$ sec) measurements. We have chosen this sample because the single crystals with this Pr concentration are at the crossover region of the phase diagram discussed above, as marked with an arrow in Fig. 1. Therefore they could display different competing orders. Specifically, in this region SC could coexist with the AFM glassy state of both Cu and Pr sublattices. Indeed, we have found that the paramagnetic state is not a trivial one, but displays a rich behavior including irreversibility and strong superconducting fluctuations in a certain domain of the H - T space.

II. EXPERIMENTAL DETAILS

The $Y_{0.47}Pr_{0.53}Ba_2Cu_3O_{7-\delta}$ single crystal, which data are presented here, of size $0.77 \times 0.57 \times 0.067$ mm³, was grown using a standard procedure described elsewhere²⁰ and was submitted to a complex magnetic investigation: magnetization M vs magnetic field H , and dc- and ac-magnetization vs temperature measurements. These measurements were performed with a superconducting quantum interference device (SQUID) magnetometer. The single crystal was mounted on a Teflon support, which was submitted to the same investigations as the sample in order to subtract the background contribution of the Teflon from the measured signal. Each run was performed after the single crystal was warmed up to temperatures higher than 200 K and cooled in zero-magnetic field down to the temperature of investigation. In some cases, different protocols were applied for field sweep as described below. In all cases, the field was applied perpendicular to the ab plane of the single crystal. The sample has a critical temperature $T_c = 13$ K as obtained from ac-susceptibility measurements.

For comparison, we also measured the temperature dependence of the resistivity. We attached four gold wires (0.025 mm in diameter) with silver epoxy onto each of the two large faces of the single crystal. A constant current $I \leq 1$ mA was fed alternately on both faces, and the voltage on each face of the single crystal was measured at set temperatures between 1.9 and 300 K. The out-of-plane ρ_c and in-plane ρ_{ab} resistivities were calculated using an algorithm described elsewhere.²¹ The critical temperature, taken at the midpoint of the normal-superconductor transition, was also found to be 13 K.

III. RESULTS AND DISCUSSION

Figure 2 shows the magnetization M vs applied magnetic field H measured at 2 K. The hysteresis loop is typical for superconducting systems coexisting with local paramagnetic moments. Therefore we assume that the magnetization loop is the superposition of a typical superconducting magnetization and a Brillouin function describing the paramagnetic moments. In order to check the correctness of this assumption, we investigated the low field dependence of the magnetization, $-900 \leq H \leq 900$ Oe, at temperatures high above the critical temperature where a paramagnetic behavior due

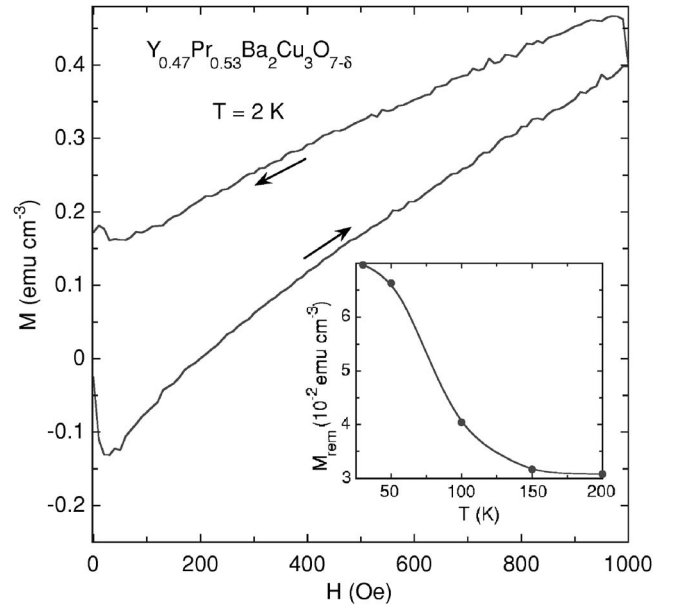


FIG. 2. Magnetization M vs applied magnetic field H measured at 2 K in increasing and decreasing magnetic field up to 1 kOe. Inset: Temperature T dependence of the remanent magnetization M_{rem} .

to Pr and Cu ions is expected. Surprisingly, the hysteresis loops survive up to temperatures as high as 200 K.

Figures 3(a)–3(d) show the evolution of the magnetization from temperatures below T_c [Fig. 3(a)] up to 200 K [Fig. 3(d)]. The remanent magnetization, defined as the width of the hysteresis curve at $H=0$, decreases fast with increasing T (see inset of Fig. 2). At high temperatures or magnetic fields, the magnetization loops show a small tendency to saturation, like in the case of ferrimagnetic materials. At even higher applied magnetic fields, the magnetization becomes reversible but it starts to deviate from linearity in a sublinear way (see Fig. 4), which is more conspicuous at low temperatures.

There could be several reasons responsible for the above discussed irreversibility for $T_c < T \leq 200$ K. For example, one could associate this irreversibility with a history dependent antiferromagnetic domain structure, like in the case of site-diluted antiferromagnets.²² However, 200 K is close to the Néel temperature T_N^{Cu} for the pure $PrBa_2Cu_3O_{7-\delta}$, which makes this assumption less plausible. Additionally, the fact that the deviation of $M(H)$ from linearity is small indicates that the paramagnetic state is dominant in this temperature range. The sublinearity noticed at high fields suggests that the reason for the hysteretic behavior of $M(H)$ could be the existence of some magnetically ordered “objects” with an internal magnetic structure, embedded in a paramagnetic “sea.” Hence with increasing magnetic field, these objects orient along the magnetic field and their total magnetic moment evolves toward saturation. One would expect that the number of these magnetic entities decreases with increasing temperature and, finally, they disintegrate as free moments. This evolution would explain the fast decrease of the remanent magnetization with increasing T (see inset of Fig. 2).

For a further insight into the magnetic response, we investigated the temperature dependence of the dc susceptibility

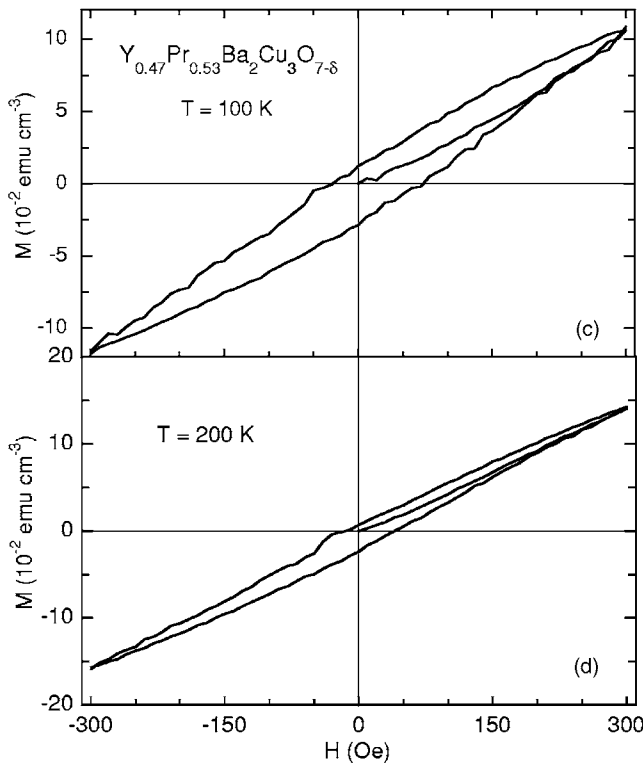
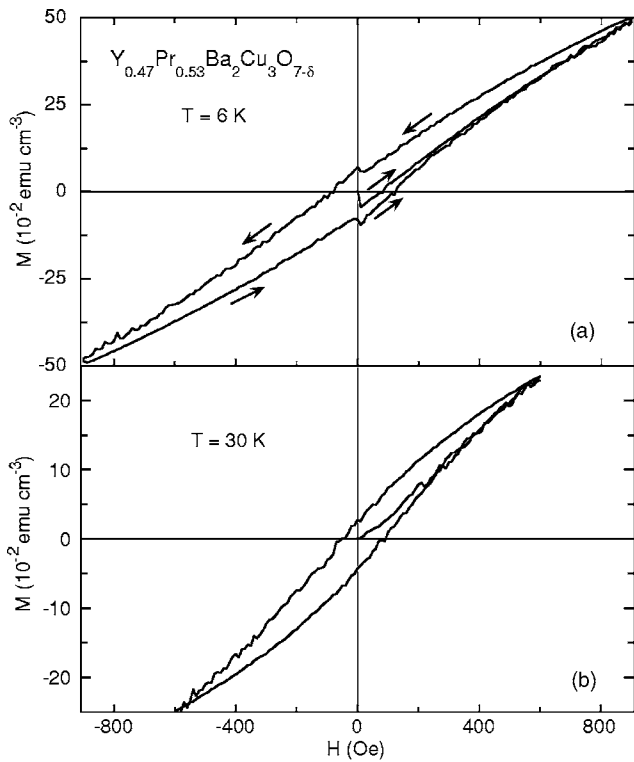


FIG. 3. Magnetization M vs applied magnetic field H measured at four different temperatures in increasing and decreasing magnetic field.

ity χ for several applied magnetic fields. As shown by Fig. 5 a general feature is the strong field dependence of the susceptibility. This effect is not present in $Y_{1-x}Pr_xBa_2Cu_3O_{7-\delta}$ with low x values, i.e., close to the optimal doping, and is

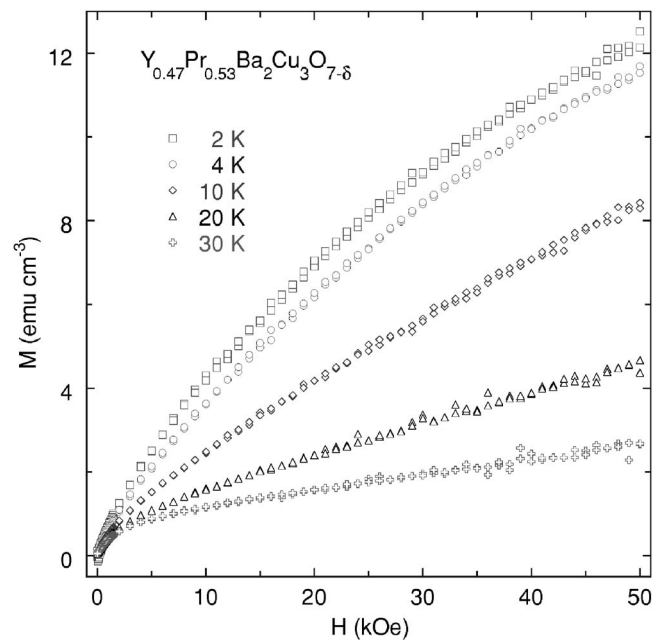


FIG. 4. Magnetization M vs applied magnetic field H measured at several temperatures.

contrary to the standard paramagnetic behavior. For $H \leq 400$ Oe, all the curves display irreversibility, i.e., a difference between zero-field-cooled χ_{ZFC} and field-cooled χ_{FC} susceptibilities, which, at low applied magnetic fields, extends far above 100 K.

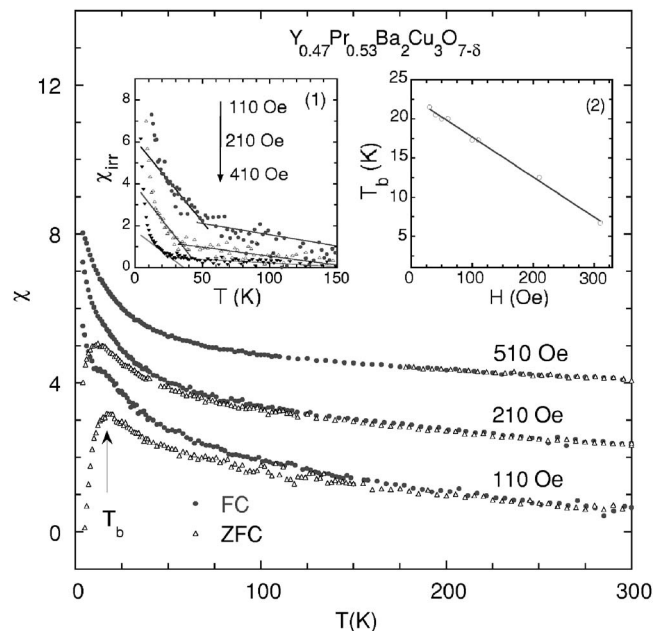


FIG. 5. Temperature T dependence of the dc susceptibility χ shown for three different applied magnetic fields. Inset: (1) Temperature T dependence of irreversible susceptibility $\chi_{irr} \equiv (\chi_{FC} - \chi_{ZFC})/2$. The solid lines are guides to the eye. (2) Linear magnetic field H dependence of the temperature T_b at which the zero-field-cooled magnetization displays a maximum. The solid line is a linear fit of the data.

The zero-field-cooled susceptibility χ_{ZFC} is negative at low temperatures and low fields, in agreement with the expected diamagnetic screening in the superconducting state. At higher temperatures, χ_{ZFC} becomes positive, exhibits a wide maximum, and then decreases with further increasing T , following a Curie-Weiss (CW) law. The field-cooled susceptibility χ_{FC} is monotonic with T and displays two temperature dependences. At high temperatures, it follows a CW temperature dependence for any value of the magnetic field, with parameters slightly different than the ones obtained from the $\chi_{ZFC}(T)$ dependence. Below the temperature corresponding approximately to the peak in the zero-field-cooled susceptibility, $\chi_{FC}(T)$ changes its behavior, roughly following a $T^{-\alpha}$ dependence with α increasing with increasing field up to $\alpha \approx 0.5$. Above 300 Oe, the transition between this T dependence at low T and the CW dependence at high T is smeared out and becomes visible only in the derivative of $\chi_{FC}(T)$.

As a general feature, the hysteretic behavior can be divided into two regimes (inset 1 to Fig. 5): At low temperatures, there is a large irreversibility $\chi_{irr} \equiv (\chi_{FC} - \chi_{ZFC})/2$, which also shows a strong T dependence, i.e., χ_{ZFC} and χ_{FC} display completely different T dependences; at higher temperatures the irreversibility is small with a weak T dependence, with both $\chi_{ZFC}(T)$ and $\chi_{FC}(T)$ displaying a CW T dependence, i.e.,

$$\chi = \chi_0 + \frac{C}{T - \theta}, \quad (1)$$

with slightly different parameters. Here, χ_0 includes the Pauli and Van Vleck paramagnetism, as well as the core diamagnetism,²³ $C = p_{eff}^2 \mu_B^2$ is the Curie-Weiss constant, related to the effective Bohr magneton number, and θ is the Curie temperature.

On one hand, such a CW temperature dependence implies the existence of free moments in the irreversible regime. On the other hand, a history dependent paramagnetism is not consistent with one arising from ionic magnetic moments, but from magnetic moments having an internal structure, which depends on field and the measuring protocol. A fit of both $\chi_{ZFC}(T)$ and $\chi_{FC}(T)$ with a CW law provides field-dependent χ_0 , C , and θ . All these parameters decrease with increasing H , another behavior which rules out the ordinary paramagnetism.

Since the CW parameters obtained from $\chi_{ZFC}(T)$ and $\chi_{FC}(T)$ are slightly different, as discussed above, with the ZFC parameters almost always larger than the FC parameters, we chose to obtain the CW parameters in this T range using the reversible susceptibility defined as $\chi_{rev} = (\chi_{ZFC} + \chi_{FC})/2$. The validity of the CW dependence of $\chi(T)$ is shown by the linearity of the χ_{rev} vs $(T + \theta)^{-1}$ plot (inset 1 of Fig. 6). The CW parameters θ_{rev} and C_{rev} follow a power-law field dependence, i.e., $C \propto H^{-\gamma}$ and $\theta \propto H^{-\beta}$, at low fields ($H \leq 500$ Oe) with $\gamma \approx 0.58$ and $\beta \approx 2/3$ (Fig. 6), whereas χ_{0rev} decreases linearly with increasing field (inset 2 of Fig. 6).

The ac-susceptibility measurements show a clear diamagnetic signal (Fig. 7), which is almost linear in T for $T_c < T$

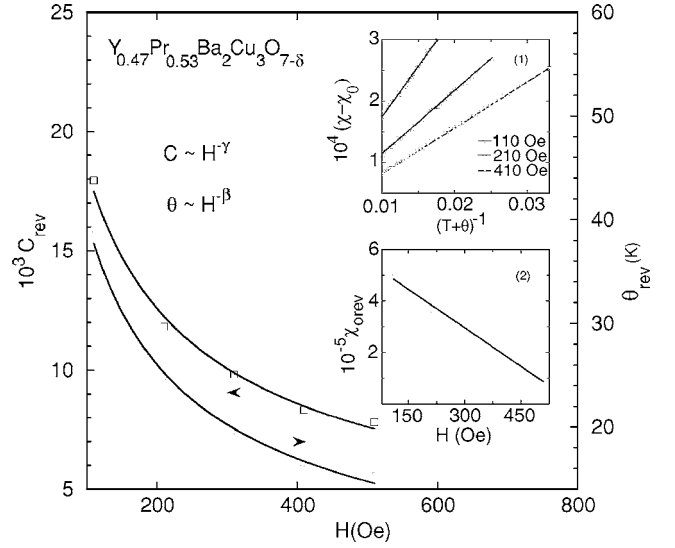


FIG. 6. Magnetic field H dependence of the Curie-Weiss parameters C and θ (main panel), and χ_0 [inset (2)]. Inset (1): Reversible susceptibility χ_{rev} vs $(T + \theta_{rev})^{-1}$. The solid lines are linear fits of the data.

≤ 200 K. We attribute this diamagnetic signal above T_c to strong superconducting fluctuations, most likely phase fluctuations. The contribution of the glassy state is not visible in these measurements because, usually, it displays a flat response if the frequency of the ac field is far from the characteristic frequency.

Diamagnetic regions at much higher temperatures than the critical temperature were first reported in SQUID microscopy measurements on underdoped $\text{La}_{2-x}\text{Sr}_x\text{CuO}_4$ single crystals.²⁴ Diamagnetism above T_c in ac susceptibility has already been reported in almost optimally doped

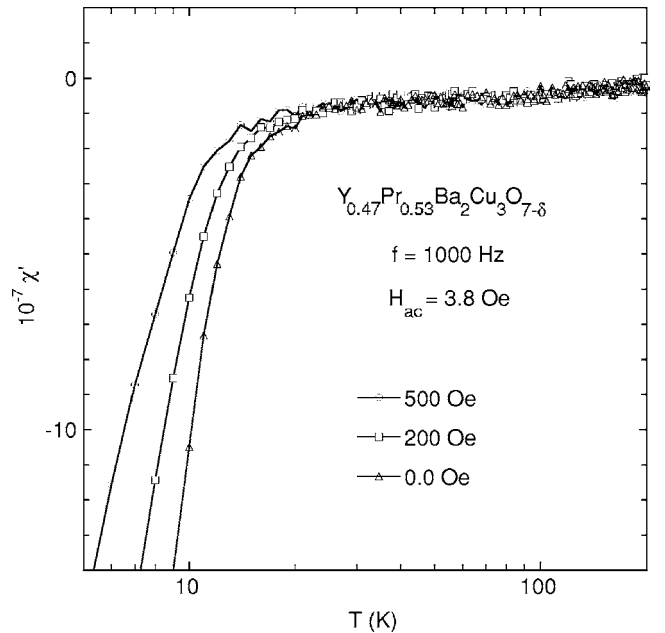


FIG. 7. Temperature T dependence of the ac susceptibility χ' measured in an ac magnetic field $H_{ac} = 3.8$ Oe and a frequency $f = 1000$ Hz.

$La_{2-x}Sr_xCuO_4$ in the same geometry as the one in the present investigation.²⁵ Their thermal investigations have confirmed that the source of the signal is the transverse fluctuations of the phase of the order parameter, as has been predicted by Emery and Kivelson.^{26,27}

An attempt to understand the above experimental data has to be based on the changes induced by Pr into the $YBa_2Cu_3O_{7-\delta}$ cuprate, as well as the NMR, μ SR, and neutron-scattering data available for other superconducting cuprates at the edge of the superconducting to Mott insulator transition. The role played by Pr doping on $YBa_2Cu_3O_{7-\delta}$ is depicted by the phase diagram of Fig. 1. The dilution of Pr ions with decreasing x from 1 toward the critical value $x_c \approx 0.55$ reduces both the Pr-Pr AFM exchange energy and the degree of f - p hybridization, which in turn decreases the Néel temperature of both Cu and Pr subsystems. The holes become itinerant and enhance the competition between long-range and short-range interactions. As a result, the AFM long-range order breaks down,^{27,28} spin randomness becomes favorable,²⁹ and superconducting *puddles*, i.e., microscopic regions with a finite superconducting order parameter but which are not phase correlated, appear.³⁰

Since the present magnetic investigations cannot provide information on the type of spin randomness, we assume, based on μ SR, neutron-scattering, and NMR data obtained on strongly underdoped but superconducting $La_{1-x}Sr_xCuO_4$ and $YBa_2Cu_3O_{6+x}$, that there is charge and spin separation in the present underdoped cuprate. When the spin randomness is a result of phase separation, it is associated with border domains, i.e., ant domain walls (ADWs), over which a change in the orientation of the staggered magnetization occurs.³¹ These ADW's accumulate the frustration induced by charge doping hence carry a finite magnetic moment and provide favorable channels for hole motion³² and pairing. Therefore within this model, for Pr concentrations below x_c , the superconducting *puddles* correlate their phase either through percolation or through Josephson coupling, giving rise to bulk superconductivity.

With increasing T , this glassy system changes into a viscous "liquid," i.e., droplets with antiferromagnetically ordered cores "floating" in a paramagnetic *sea*. Even though the density of the magnetic droplets decreases with further increasing T , they most likely survive beyond the bulk Néel temperature, as evidenced by the irreversibility present in the $M(T)$ data. As shown below, these long lasting droplets behave like superparamagnetic particles with an antiferromagnetic core and a magnetic shell corresponding to the frustrated spin region. In fact, Cho *et al.*³³ reported fluctuations of the staggered magnetization in the high-temperature La^{139} NQR spin-lattice relaxation rate of $La_{1-x}Sr_xCuO_4$ that is reminiscent of the superparamagnetic relaxation.

The above proposed model is consistent with the field and temperature dependence of the measured dc magnetization which, presumably, consists of superconducting, glassy, and paramagnetic contributions. Indeed, the low-temperature data (Fig. 2) show that in the ZFC $M(H)$ protocol, the diamagnetic screening is effective at low fields. With increasing magnetic field, the field penetrates in the form of vortices, which are extended because of the large penetration depth. In the framework on the proposed model, the magnetic droplets

start to feel the presence of the magnetic field, thus contributing to the total magnetization. The stronger the magnetic field the stronger their contribution becomes, which would explain the increase of the total magnetization with increasing H . However, the increase is sublinear, with a salient tendency to saturation at high fields, most likely due to the alignment of the magnetic moments of the ADW's (shells) with the magnetic field (Fig. 4).

The $M(T)$ data are also consistent with the proposed core-shell model. In the superconducting state, starting from low temperatures and at fields up to 400 Oe, the response is diamagnetic, i.e., $\chi < 0$ (Fig. 5). Also, the trapped field in the mixed state as well as the nonergodicity due to the large number of metastable states, typical for any kind of glassy state, give rise to a difference between the FC and ZFC magnetizations. At temperatures above T_c , the superconducting contribution is reduced to an only negligible fluctuating diamagnetism (nevertheless visible in ac susceptibility), the droplet contribution is also weakened, hence the pure paramagnetic contribution becomes dominant. The extra paramagnetism due to the moments of the surviving droplets gives rise to a weak irreversibility, i.e., a small difference between FC and ZFC of both $M(T)$ (Fig. 5) and $M(H)$ [Figs. 3(b)–3(d)].

The magnetic moment of the shells, as in the case of superparamagnetic particles, shows a maximum in the ZFC $M(T)$ at a certain field-dependent temperature T_b (Fig. 5), which is the equivalent of the blocking temperature in superparamagnetic systems. In the latter systems, the blocking temperature is proportional to the energy barrier between degenerate states. The maximum in $M(T)$ is the result of the competition between the Zeeman energy (which lifts this degeneracy by adding a $\pm\mu\mathbf{H}$ term) of the unfrozen droplets, which align along the applied magnetic field, and the thermal energy, which tends to randomize the moments hence to decrease $M(T)$ in a Curie-Weiss way. The peak in $M(T)$ is rather broad probably because of a distribution of the blocking temperatures in this system. At low fields, T_b decreases linearly with H (inset 2 of Fig. 5); i.e.,

$$T_b(H) = T_b(0) \left(1 - \frac{H}{H_0} \right), \quad (2)$$

with $T_b(0) = 22.8$ K and $H_0 = 445$ Oe.

The power-law T dependence of the field-cooled susceptibility for $T < T_b$, i.e., $\chi_{FC} \propto T^{-\alpha}$, could also be attributed to the frustration, which generates magnetic moment. At these temperatures, the flipped spin passes into the wall increasing the wall size. Therefore the exponent α increases with increasing field. A similar effect was reported in superparamagnetic systems with antiferromagnetic cores.³¹ An alternative explanation for the increase of the spin susceptibility below T_c has been given by Ohashi who has proposed an increase in the density of electronic states due to the generation of low-energy states around impurities.³⁴ This increase in turn enhances the AFM spin fluctuations, which produce an increase in the susceptibility as the temperature decreases.

The negative Curie-Weiss temperature θ indicates that, on average, the dominant spin-spin interaction is of AFM type.

This result could reflect the AFM nature of the droplet cores. In addition, the decrease of C with increasing H (Fig. 6) could be a result of the fact that the average magnetic moment of the droplet, which is proportional to \sqrt{C} , decreases with increasing field. Indeed, it has been shown that H influences strongly the internal structure of the droplets by flipping the spins and reducing their exchange constant.³⁵

IV. SUMMARY

In conclusion, we find that the magnetic behavior of $Y_{0.47}Pr_{0.53}Ba_2Cu_3O_{7-\delta}$ is very complex. The magnetization data suggest the coexistence of superconductivity and glassy magnetism at low temperatures. The high-temperature regime of the system has been interpreted as consisting of a

paramagnetic background, superconducting phase fluctuations, and remnants of the glassy state as droplets with an antiferromagnetic core that coexist up to very high temperatures (200 K). The latter is responsible for the high-temperature irreversibility. We propose a core-shell model for the contribution of the clusters, which is consistent with all the present data.

ACKNOWLEDGMENTS

This research was supported by the National Science Foundation under Grant No. DMR-0406471 at KSU and the U.S. Department of Energy under Grant No. DE-FG02-04ER46105 at UCSD.

*Permanent Address: National Institute of Materials Physics, 077125 Bucharest-Magurele, Romania.

¹B. Keimer, N. Belk, R. J. Birgeneau, A. Cassanho, C. Y. Chen, M. Greven, M. A. Kastner, A. Aharony, Y. Endoh, R. W. Erwin, and G. Shirane, *Phys. Rev. B* **46**, 14034 (1992).

²F. C. Chou, N. R. Belk, M. A. Kastner, R. J. Birgeneau, and A. Aharony, *Phys. Rev. Lett.* **75**, 2204 (1995).

³S. Wakimoto, S. Ueki, Y. Endoh, and K. Yamada, *Phys. Rev. B* **62**, 3547 (2000).

⁴F. Cordero, A. Paolone, R. Cantelli, and M. Ferretti, *Phys. Rev. B* **62**, 5309 (2000).

⁵C. Panagopoulos and V. Dobrosavljević, *Phys. Rev. B* **72**, 014536 (2005).

⁶Ch. Niedermayer, C. Bernhard, T. Blasius, A. Golnik, A. Moodenbaugh, and J. I. Budnick, *Phys. Rev. Lett.* **80**, 3843 (1998).

⁷M.-H. Julien, F. Borsa, P. Carretta, M. Horvatić, C. Berthier, and C. T. Lin, *Phys. Rev. Lett.* **83**, 604 (1999).

⁸M.-H. Julien, A. Campana, A. Rigamonti, P. Carretta, F. Borsa, P. Kuhns, A. P. Reyes, W. G. Moulton, M. Horvatić, C. Berthier, A. Vietkin, and A. Revcolevschi, *Phys. Rev. B* **63**, 144508 (2001).

⁹G. Shirane, J. Als-Nielsen, M. Nielsen, J. M. Tranquada, H. Chou, S. Shamoto, and M. Sato, *Phys. Rev. B* **41**, 6547 (1990).

¹⁰H. Chou, J. M. Tranquada, G. Shirane, T. E. Mason, W. J. L. Buyers, S. Shamoto, and M. Sato, *Phys. Rev. B* **43**, 5554 (1991).

¹¹Y. Ando, A. N. Lavrov, and K. Segawa, *Phys. Rev. Lett.* **83**, 2813 (1999).

¹²M. Sutherland, S. Y. Li, D. G. Hawthorn, R. W. Hill, F. Ronning, M. A. Tanatar, J. Paglione, H. Zhang, L. Taillefer, J. DeBenedictis, R. Liang, D. A. Bonn, and W. N. Hardy, *Phys. Rev. Lett.* **94**, 147004 (2005).

¹³S. Sanna, G. Allodi, G. Concas, A. D. Hillier, and R. De Renzi, *Phys. Rev. Lett.* **93**, 207001 (2004).

¹⁴Y. Sidis, C. Ulrich, P. Bourges, C. Bernhard, C. Niedermayer, L. P. Regnault, N. H. Andersen, and B. Keimer, *Phys. Rev. Lett.* **86**, 4100 (2001).

¹⁵C. Stock, W. J. L. Buyers, Z. Yamani, C. L. Broholm, J.-H. Chung, Z. Tun, R. Liang, D. Bonn, W. N. Hardy, and R. J. Birgeneau, *Phys. Rev. B* **73**, 100504(R) (2006).

¹⁶I. Felner, U. Yaron, I. Nowik, E. R. Bauminger, Y. Wolfus, E. R. Yacoby, G. Hilscher, and N. Pillmayr, *Phys. Rev. B* **40**, 6739 (1989).

¹⁷A. Kebede, C. S. Jee, J. Schwegler, J. E. Crow, T. Mihalisin, G. H. Myer, R. E. Salomon, P. Schlottmann, M. V. Kuric, S. H. Bloom, and R. P. Guertin, *Phys. Rev. B* **40**, 4453 (1989).

¹⁸D. W. Cooke, R. S. Kwok, R. L. Lichti, T. R. Adams, C. Boekema, W. K. Dawson, A. Kebede, J. Schwegler, J. E. Crow, and T. Mihalisin, *Phys. Rev. B* **41**, 4801 (1990).

¹⁹T. Katuwal, V. Sandu, C. C. Almasan, B. J. Taylor, and M. B. Maple, *Phys. Rev. B* **72**, 174501 (2005).

²⁰L. M. Paulius, B. W. Lee, M. B. Maple, and P. K. Tsai, *Physica C* **230**, 255 (1994).

²¹G. A. Levin, T. Stein, C. N. Jiang, C. C. Almasan, D. A. Gajewski, S. H. Han, and M. B. Maple, *Physica C* **282–287**, 1147 (1997).

²²Y. Kim and A. B. Harris, *Phys. Rev. B* **32**, 4676 (1985).

²³W. C. Lee and D. C. Johnston, *Phys. Rev. B* **41**, 1904 (1990).

²⁴I. Iguchi, A. Sugimoto, T. Yamaguchi, N. Chaki, T. Miyake, I. Tanaka, and S. Watauchi, *Physica C* **367**, 9 (2002).

²⁵U. Thisted, J. Nyhus, T. Suzuki, J. Hori, and K. Fosshem, *Phys. Rev. B* **67**, 184510 (2003).

²⁶V. J. Emery and S. A. Kivelson, *Nature (London)* **374**, 434 (1995).

²⁷V. J. Emery, S. A. Kivelson, and O. Zachar, *Phys. Rev. B* **56**, 6120 (1997).

²⁸V. J. Emery and S. A. Kivelson, *Physica C* **209**, 597 (1993); *Synth. Met.* **80**, 151 (1996).

²⁹J. Schmalian and P. G. Wolynes, *Phys. Rev. Lett.* **85**, 836 (2000).

³⁰G. Alvarez, M. Mayr, A. Moreo, and E. Dagotto, *Phys. Rev. B* **71**, 014514 (2005).

³¹R. N. Bhowmik, R. Nagarajan, and R. Ranganathan, *Phys. Rev. B* **69**, 054430 (2004).

³²D. Poilblanc and T. M. Rice, *Phys. Rev. B* **39**, 9749 (1989).

³³J. H. Cho, F. Borsa, D. C. Johnston, and D. R. Torgeson, *Phys. Rev. B* **46**, 3179 (1992).

³⁴Y. Ohashi, *Phys. Rev. B* **66**, 054522 (2002).

³⁵K. Yosida, *Theory of Magnetism*, Springer Series in Solid State Science Vol. 122 (Springer-Verlag, Berlin, 1998), p. 76.